International Journal of Mechanical and Electrical Engineering
ISSN: 3005-9615 (Print), ISSN: 3005-7132 (Online) | Volume 2, Number 2, Year 2024
DOI: https://doi.org/10.62051/ijmee.v2n2.12
Journal homepage: https://wepub.org/index.php/IJMEE/index

Structural Optimization and Process Scheme of Large-span Gantry Crossbeam based on Response Surface

Jiahu Zhang [1], Yun Xu [1], Shuai Ye [1], Ting Chen [1] and Hao Fang [2]

[1] School of Mechanical Engineering, Sichuan University of Science and Engineering, Zigong 643000, China

[2] Hualu Hengsheng (Jingzhou) Co., Ltd., Jingzhou, 434000, China

ABSTRACT

A comprehensive design method for large-span gantry beams, combining process techniques and structural optimization, is proposed to address significant deflection deformation issues caused by their own gravity and the gravity of front attachments. Selecting the beam section type, finite element static analysis is performed using ANSYS Workbench for both cast and welded gantry beams. The maximum static deformation values of the beams for both process schemes are compared to determine the process scheme for the large-span beam. Subsequently, multiple structural dimensions of the welded gantry beam are parameterized, and sensitivity analysis is conducted to determine the degree of influence of each parameter on the optimization objective. Parameters with relatively small effects on the corresponding objectives are eliminated. A response surface multi-objective genetic algorithm optimization based on Box-Behnken design experimental design method is employed to minimize deflection deformation and reduce weight. The response surface model is fitted with expressions, and variance and significance analyses are conducted to validate the model's reliability. The optimal Pareto solutions are determined based on the response surface model using a multi-objective genetic algorithm. A comparison between the beams before and after optimization shows a reduction of 0.052 in maximum static deformation of the welded beam, representing an 8.3% decrease. Additionally, the mass decreases by 1710 kg, indicating a 14.63% reduction, demonstrating significant optimization effects.

KEYWORDS

Crossbeam Section; Response Surface Model; Significance Analysis; Multi-objective Optimization.

1. INTRODUCTION

In the design of modern large-scale machining equipment, the gantry-type structure is often chosen as the preferred option for heavy and large-scale machinery. The gantry-type machine tool structure is capable of meeting the machining requirements of massive volumes and longitudinally lengthy parts. Within the gantry structure, the beam holds the largest proportion and is the most crucial load-bearing component, being the focal point of machine tool overall structural design and optimization. As the span of the beam increases, deflection deformation is induced in the gantry-type beam due to the effects of its own gravity and the gravity of front attachments, resulting in adverse effects on the laying accuracy of the machine tool.

From the perspective of beam manufacturing processes, traditional beams are typically formed through casting. However, with the increase in beam size, the electric furnaces and molds used in casting cannot meet the casting requirements of the beams. Li Zhongtian [1] adopted a welding process to manufacture the beams. Through finite element analysis comparing the dynamic and static

characteristics of welded and cast beams, the results showed that under equal quality conditions, the stiffness of welded beams is superior to that of cast beams, suggesting that the welding process is a preferable method for beam manufacturing. Research revolves around methods to increase beam stiffness by optimizing beam structures. Zatarain et al. [2] studied various approaches to increase beam stiffness using different optimization methods and verified the reliability of methods to enhance beam stiffness, providing valuable recommendations for improving beam stiffness. Li et al. [3] utilized finite element analysis to conduct structural topology optimization of gantry-type grinding machine beams, reducing the maximum stress and deformation of gantry beams. Guo Linna et al. [4], based on the finite element method, conducted static and dynamic analysis of beams in a gantry machining center, converting the cross-shaped reinforcement structure into a T-shaped one, thereby improving the deformation and first-order natural frequency of the gantry beam. Optimizing the structure can increase the overall stiffness of the beam and reduce errors. This paper combines process techniques and structural optimization methods to comprehensively design large-span gantry beams. Two process schemes, welding, and casting, are adopted for large-span beams. Finite technology is utilized to compare the maximum static deformation of the two types of beams under the same conditions. Sensitivity analysis of beam structural parameters is conducted, and multi-objective response surface optimization is performed on welded beam structures to obtain optimized results. This comprehensive design approach provides guidance for the design of similar types of machine tool structures.

2. CROSSBEAM SECTION DESIGN

The commonly used traditional gantry beam section shapes are illustrated in Figure 1. Among them, structures (1)-(3) represent the most widely applied beam section type - rectangular, while structures (4)-(6) are variants derived from the traditional rectangular section, referred to as irregular section beams. The advantage of the rectangular section structure lies in its simple section shape, facilitating the theoretical calculation of various beam performance indicators such as moment of inertia, bending section modulus, and torsional section modulus. According to theoretical mechanics knowledge, when the ratio of width to length of the rectangular section is, the beam's bending stiffness is optimal. In the case of the same cross-sectional area, the bottom dimension of the irregular section is enlarged, thereby increasing the beam's moment of inertia. Structure (6) is an improvement upon (3), where the section shape changes from a rectangle to a quadrilateral with slanted edges. The inclination angle of the slanted surface can be adjusted according to the loading condition of the moving components, improving the beam's load-bearing stiffness [5].

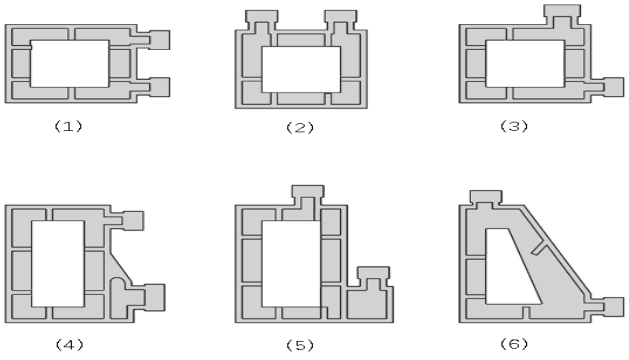

Figure 1. Cross-sectional structure of a beam

3. FINITE ELEMENT STATIC ANALYSIS OF WELDED AND CAST CROSSBEAMS

3.1. Crossbeam Manufacturing Scheme

In the field of large-scale machine tool manufacturing, beam blanks can currently be prepared using two manufacturing processes: welding and casting.

Each of these processes has its own advantages and disadvantages. Castings exhibit stronger vibration absorption properties than welded components and are superior in residual stress treatment. Casting also requires the production of wooden molds, which, when available, can quickly expand production scale. However, drawbacks are also associated with wooden molds, as casting may result in defects such as gas holes and sand eyes, necessitating continuous adjustment of the molds. Additionally, when there are changes in the beam structure, the existing wooden molds become obsolete, requiring remaking, leading to significant waste of resources and increasing development costs, thus posing challenges for product modification.

On the other hand, welded components require simpler manufacturing equipment, shorter production cycles, and easy modification. However, the quality of welded components is closely related to process arrangements. Welding can introduce relatively high residual stresses and uncontrollable welding deformations. Under the same stiffness conditions, the weight of welded structures is only two-thirds that of cast structures, offering new ideas for light weighting large and heavy machine tool components and creating conditions for high-speed operation of large machine tools.

3.2. Comparative Analysis of Static Performance.

(1) Establishing a three-dimensional model and simplification of the beam.

The dimensions of the cast beam in length, width, and height are 12×1.2×1.5m. Using SolidWorks three-dimensional software, a three-dimensional solid model of the beam is constructed according to existing drawings.

To improve computational efficiency and accuracy, it is necessary to simplify the solid model. This involves disregarding all minor features such as small holes, chamfers, fillets, lubrication grooves, bosses, etc., in the three-dimensional model. To reflect the differences in manufacturing processes, the pouring holes on the cast beam are retained, while the wall panels of the welded beam are not drilled, and instead, a single steel plate is used.

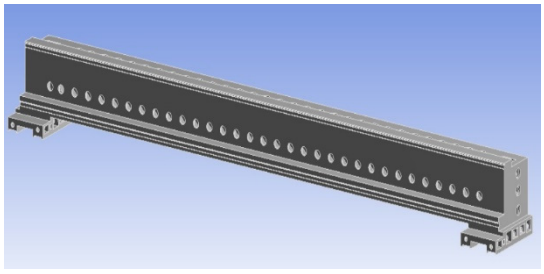

Figure 2. Simplified model of a cast beam

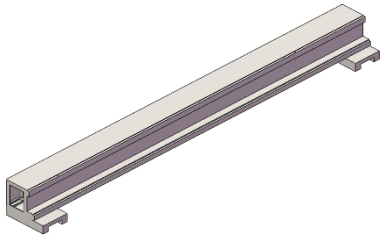

Figure 3. Simplified model of welded beam

The simplified and modified models are shown in Figures 2 and 3. The outer dimensions of the welded beam are the same as those of the cast beam. However, due to the different requirements of casting and welding processes, the arrangement of stiffeners on the welded beam cannot be the same as that of the traditional cast structure. On one hand, this is to avoid excessive and concentrated welding

seams on the beam, which would result in high welding stresses and severe welding deformations, thus reducing the structural stability of the beam. On the other hand, the manufacturing process of the welded beam is not constrained by the fluidity of molten iron, allowing for the selection of steel plates of different thicknesses according to the strength requirements of different locations. This approach ensures structural rigidity while saving materials and reducing costs. The welded beam is composed of top plates, web plates, rib plates, reinforcing ribs, etc., welded together, forming an L-shaped cross-section.

The simplified models are saved as x-t files and imported into ANSYS Workbench.

(2) Material definition and mesh partitioning.

The cast structure adopts gray cast iron HT250, For the various steel plates of the welded components, contact pairs are established, and the material is set as Q345A, with detailed parameters provided in Table 1. The default solid element type of ANSYS Workbench is used, and a Hex Dominant mesh control is employed to generate hexahedral meshes.

Table 1. Material Data Table

material name.	HT250	Q345A
density. (kg/m^3)	7250	7800
elastic modulus. E (Pa)	$1.3x10^{11}$	$2.1x10^{11}$
poisson's ratio.	0.27	0.3

(3) Loading and constraint application

The standard earth gravity (gravity acceleration) is applied to simulate the gravity of the beam and the moving parts on it. A fix support (full displacement constraint) is applied to the slider position at the base of the beam.

(4) Finite element calculation results and data analysis

The finite element model of the beam is solved using Workbench, and the total displacement cloud maps and displacement cloud maps in each direction for both schemes are examined. See Table 2 for details.

(1) Both the cast and welded gantry beams simultaneously bear the effects of gravity, tension, and bending moments. Concerning total displacement, the maximum deformation positions for both are symmetrically located at the bottom of the beam's central symmetry plane. When stress levels are the same, materials with higher elastic moduli have higher stiffness and generate smaller strains. The elastic modulus of HT250 is smaller than that of Q345A. The maximum deformation of the cast beam is 0.91mm, while that of the welded beam is 0.72mm. The total deformation of the cast beam is approximately 1.25 times that of the welded beam.

(2) Regarding displacements in each direction, in the X-direction, the maximum displacement of the cast beam is 0.148mm, while that of the welded beam is 0.071mm. In the Y-direction, the displacement of the cast beam is 0.909mm, and that of the welded beam is 0.709mm. In the Z-direction, the maximum displacement of the cast beam is 0.049mm, while that of the welded beam is 0.114mm. It is evident that the Y and Z directions are sensitive to errors.

From the results of static analysis, it appears that the overall stiffness of the welded beam is higher than that of the cast beam.

Table 2. Deformation Cloud Maps of Cast Beam and Welded Beam

	Cast crossbeam	Welded beam
Total deformation cloud map	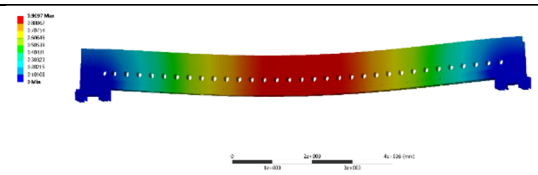	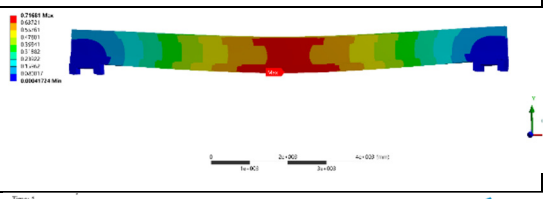
X-axis deformation cloud map	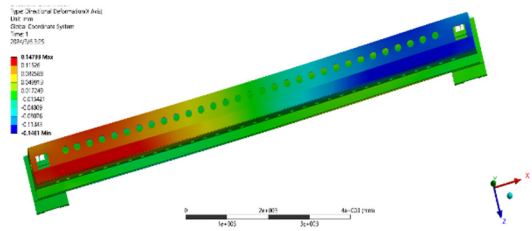	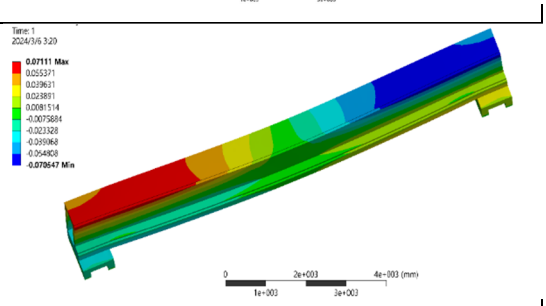
Y-axis deformation cloud map	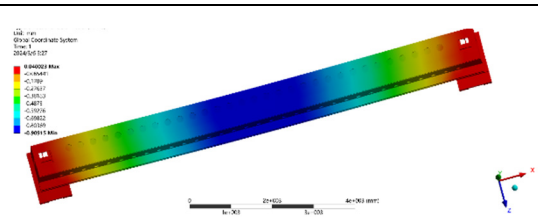	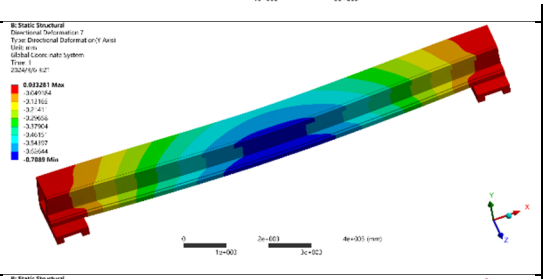
Z-axis deformation cloud map	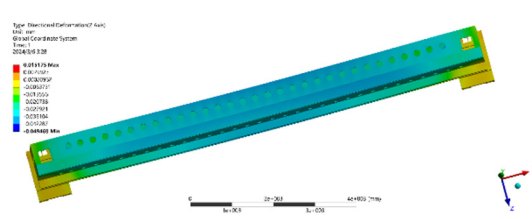	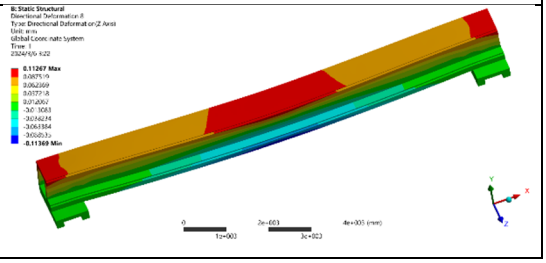

4. MULTI-OBJECTIVE RESPONSE SURFACE OPTIMIZATION OF WELDED BEAMS

Response Surface Methodology (RSM) is utilized to explore the nonlinear relationship between response variables and independent variables by designing experimental schemes and conducting a certain number of experiments using several parameters as independent variables. The corresponding response values are obtained to construct a mathematical model between them. The relationship between factors and response values is then fitted using a multivariate regression equation. The range of independent variables is narrowed down through fitting equations and contour plots. Optimal combinations of independent variables and examination of interactions are determined through numerical analysis. This relationship is then represented graphically, enabling us to intuitively select the optimal solutions and optimization areas of the experiments based on the graph [6].

4.1. Design Variables

the dimensions shown in Figure 4 are treated as design variables and parameterized. These dimensions include: bottom plate thickness (P1), stiffener plate thickness (P2), stiffener spacing (P3), overhang height (P4), overhang width (P5), section height (P6), section width (P7), main wall plate thickness (P8), and secondary wall plate thickness (P9).

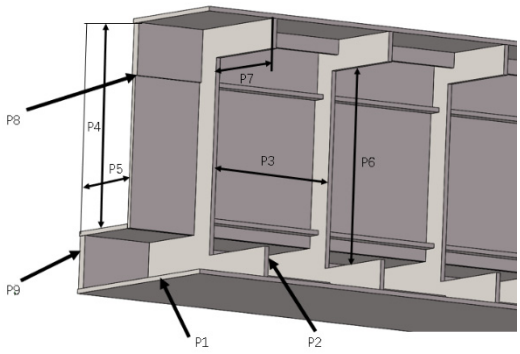

Figure 4. Variable location diagram

The range of variable values is shown in Table 3.

Table 3. Values of design variables

Variable	Initial Value	Upper Limit	Lower Limit
Bottom Plate Thickness (P1)	25	15	35
Stiffener Plate Thickness (P2)	10	8	15
Stiffener Spacing (P3)	400	300	500
Overhang Height (P4)	600	500	680
Overhang Width (P5)	200	50	300
Section Height (P6)	550	400	700
Section Width (P7)	400	330	480
Main Wall Plate Thickness (P8)	30	20	40
Secondary Wall Plate Thickness (P9)	30	20	40

4.2. Global Sensitivity Analysis

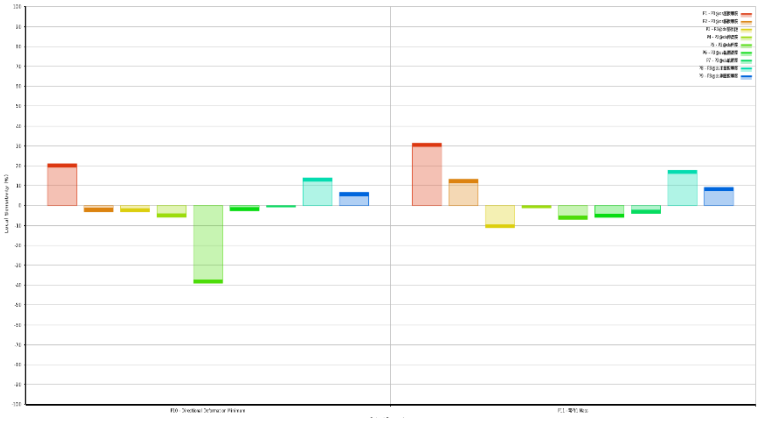

Figure 5. Column chart of parameter sensitivity

This approach can reduce the computational load during response surface construction or direct optimization processes. Taking bottom plate thickness (P1), stiffener plate thickness (P2), stiffener spacing (P3), overhang height (P4), overhang width (P5), section height (P6), section width (P7), main wall plate thickness (P8), and secondary wall plate thickness (P9) as design variables, and maximum static deformation (R1) and beam mass (R2) as response objectives, the aforementioned design variables and response parameters are parameterized. Thirty experimental sample points are

set up to determine the sensitivity of each design variable to the response objectives, as shown in Figure 5.

From the graph, it can be observed that the bottom plate thickness (P1), main wall plate thickness (P8), and secondary wall plate thickness (P9) are positively correlated with maximum static deformation, while the other design variables are negatively correlated with it. Similarly, the bottom plate thickness (P1), stiffener plate thickness (P2), main wall plate thickness (P8), and secondary wall plate thickness (P9) are positively correlated with mass, while the remaining design variables are negatively correlated with it.

Considering that the bottom plate thickness (P1), main wall plate thickness (P8), overhang width (P5), and secondary wall plate thickness (P9) have a significant impact on both response objectives, control adjustments can be made to deformation and mass by adjusting these four design variables.

4.3. Response Surface Experiment Results Analysis

Table 4. Response surface test design points and results table

Number	Floor thickness P1(mm)	Overhang width P5(mm)	Thickness of main siding P8(mm)	Thickness of secondary siding P9(mm)	Maximum static deformation P10 (mm)	P11 Part quality (kg)
1	25	175	30	30	-0.66034	11651.06
2	15	50	30	30	-0.64438	10948.66
3	35	50	30	30	-0.61144	12716.14
4	15	300	30	30	-0.73881	10585.96
5	35	300	30	30	-0.68792	12353.44
6	25	175	20	20	-0.68591	10890.34
7	25	175	40	20	-0.75956	11950.83
8	25	175	20	40	-0.67754	11351.28
9	25	175	40	40	-0.64726	12411.77
10	15	175	30	20	-0.69595	10536.85
11	35	175	30	20	-0.65549	12304.33
12	15	175	30	40	-0.68477	10997.78
13	35	175	30	40	-0.64434	12765.26
14	25	50	20	30	-0.63992	11302.16
15	25	300	20	30	-0.72572	10939.46
16	25	50	40	30	-0.61388	12362.65
17	25	300	40	30	-0.69256	11999.95
18	15	175	20	30	-0.70543	10237.07
19	35	175	20	30	-0.66613	12004.55
20	15	175	40	30	-0.67848	11297.56
21	35	175	40	30	-0.63676	13065.04
22	25	50	30	20	-0.63382	11601.94
23	25	300	30	20	-0.71114	11239.24
24	25	50	30	40	-0.61751	12062.87
25	25	300	30	40	-0.70343	11700.17

This study employs the Box-Behnken Design to design the response surface experiment plan. The sample points include four design variables: bottom plate thickness (P1), main wall plate thickness (P8), overhang width (P5), and secondary wall plate thickness (P9), totaling 25 experimental points. The design and results of the response surface experiment are shown in Table 4.

Typically, 3D outputs are used to display the relationships between various input variables and output variables, with pairs of design variables serving as the X and Y axes of the graphs, and selecting one target as the Z axis. The combinations of design variables P1 with P2, P1 with P3, P1 with P4, P2 with P3, P2 with P4, and P3 with P4 are used to plot the relationship between maximum static deformation and mass response in 3D graphs, as shown in Figures 6 and Figures 7. Through analysis of the response surface, the impact of different beam dimensions on the response values can be clearly observed.

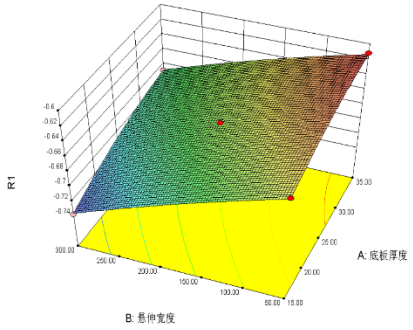

1) The response surface of maximum static deformation in relation to P1 and P2.

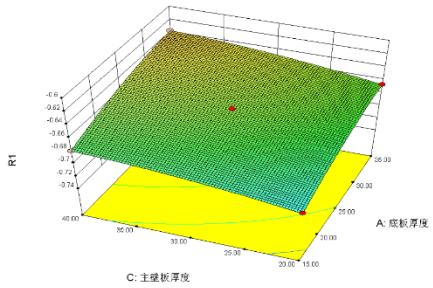

2) The response surface of maximum static deformation in relation to P1 and P3.

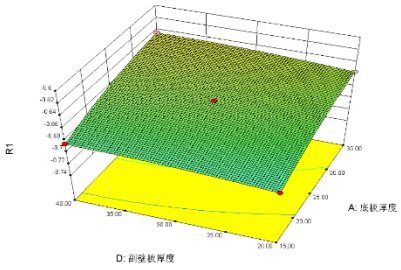

3) The response surface of maximum static deformation in relation to P1 and P4.

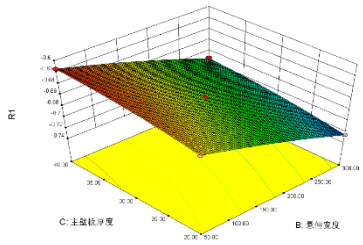

4) The response surface of maximum static deformation in relation to P2 and P3.

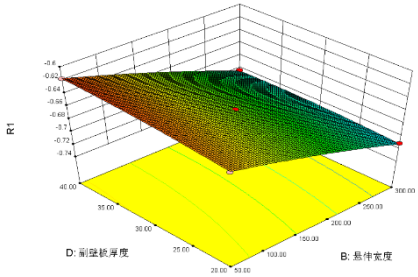

5) The response surface of maximum static deformation in relation to P2 and P4.

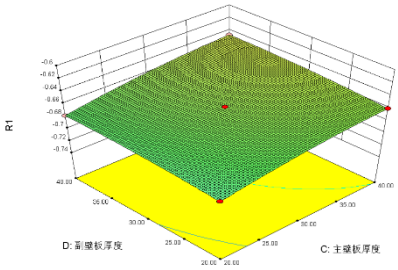

6) The response surface of maximum static deformation in relation to P3 and P4.

Figure 6. Response surface of design variable combinations to maximum static deformation

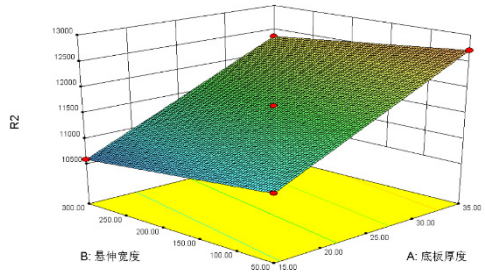

1) The response surface of mass in relation to P1 and P2.

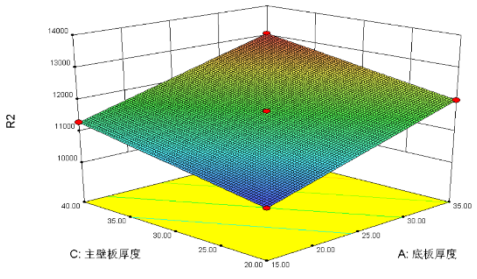

2) The response surface of mass in relation to P1 and P3.

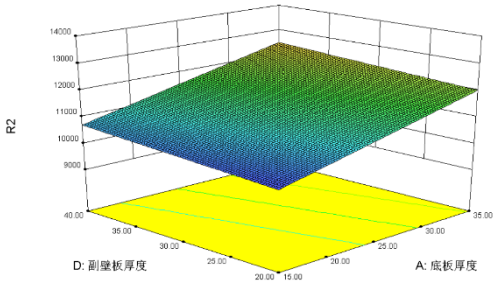

3) The response surface of mass in relation to P1 and P4.

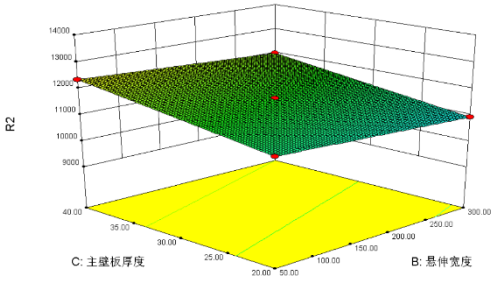

4) The response surface of mass in relation to P2 and P3.

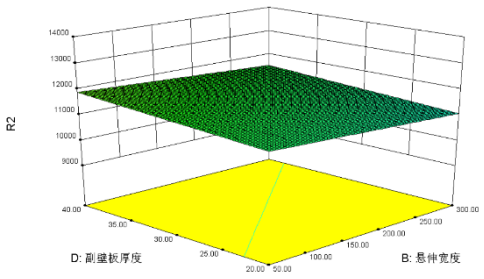

5) The response surface of mass in relation to P2 and P4.

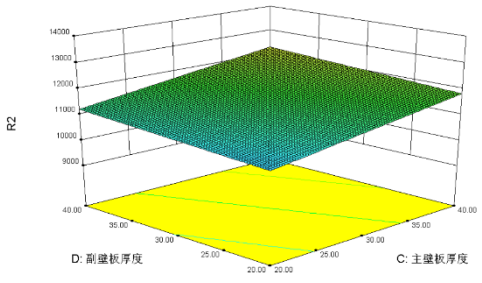

6) The response surface of mass in relation to P3 and P4.

Figure 7. Response surface diagram of design variable combinations to quality

4.4. Analysis and Significance Test of the Response Surface Regression Model for Maximum Static Deformation

Under the comprehensive influence of the selected four beam structural dimensions, the regression equation of the response surface model corresponding to the maximum static deformation is as follows (Equation 1).

$$\begin{aligned} R_1 &= -0.60073 + 4.72946\times10^{-3}\times A - 3.39247\times10^{-4}\times B + 3.37198\times10^{-3}\times C \\ &+ 2.26501\times10^{-3}\times D + 3.58968\times10^{-6}\times AB + 6.02826\times10^{-6}\times AC - 5.02169\times10^{-8}\times AD \\ &+ 1.42428\times10^{-6}\times BC - 1.71813\times10^{-6}\times BD + 9.81376\times10^{-6}\times CD - 6.97848\times10^{-5}\times A^2 \\ &- 2.11745\times10^{-7}\times B^2 - 4.38641\times10^{-5}\times C^2 - 2.83172\times10^{-5}\times D^2 \end{aligned} \quad (1)$$

4.4.1. Variance Analysis of the Regression Model for Maximum Static Deformation Response Surface

The results of the variance analysis for the maximum static deformation response surface model are shown in Table 5.

Table 5. ANOVA of the maximum static deformation-response surface regression model

Statistical evaluation index	value
Coefficient of determination ($R^{2)}$	0.9996
Correction coefficient (R_{Adj})	0.9991
Prediction coefficient (R_{pred})	0.9975
Coefficient of variation (C_v)	0.20
Measure signal-to-noise ratio (SNR)	182.772
Sum of squared prediction errors (PRESS)	7.83×10^{-5}

From the data in the table, it can be inferred that the coefficient of variation of the response surface model is relatively small, indicating that the sample data is reliable; the difference between the adequacy correction coefficient and the correction coefficient is less than 0.2, and the values are close, indicating that the regression effect of the response surface model is relatively good; the signal-to-noise ratio is greater than 4, and the sum of squared prediction errors is relatively small, indicating that the model is very accurate.

4.4.2. Significance Test for the Maximum Static Deformation Response Surface Regression Model

Significance test for the maximum static deformation response surface regression model is conducted, and the results of the test are shown in Table 6.

Table 6. Significance test table of the maximum static deformation-response surface regression model

Source	Sum of squares	Degrees of freedom	Mean square	F value	Pvalue	Significance
Model	0.029	14	2.079×10^{-3}	2334.43	< 0.0001	Highly significant
A (Bottom Plate Thickness)	5.032×10^{-3}	1	5.032×10^{-3}	5648.92	< 0.0001	Highly significant
B(Flange Width)	0.021	1	0.021×10^{-3}	23261.22	< 0.0001	Highly significant
C(Main Wall Plate Thickness)	2.469×10^{-3}	1	2.469×10^{-3}	2772.11	< 0.0001	Highly significant
D(Secondary Wall Plate Thickness)	3.743×10^{-4}	1	3.743×10^{-4}	420.14	< 0.0001	Highly significant
Residual	1.247×10^{-5}	14	8.908×10^{-7}	—	—	—
Lack of Fit	1.247×10^{-5}	10	1.247×10^{-6}	—	—	—
Pure Error	0.000	4	0.000	—	—	—
Total	0.029	28		—	—	—

Note: P<0.01 highly significant, P<0.05 significant

From the data in the table, it can be concluded that the p-value of the regression model is less than 0.005, indicating the model's significance and favorability. The F-values of the different factors in the regression model indicate the strength of their influence. The larger the F-value, the stronger the

effect. Therefore, the order of impact from greatest to least is flange width, plate thickness, main wall plate thickness, and secondary wall plate thickness.

4.5. Analysis and Significance Test of the Response Surface Regression Model for Beam Mass

Under the combined influence of the four factors of beam structural dimensions, the regression equation for the response surface model corresponding to the response value of beam mass is as follows:

$$\begin{aligned} R_2 &= 7413.4632 + 88.374 \times A - 1.4508 \times 10^{-4} \times B + 53.0244 \times C + 23.04666 \times D \\ &-2.07775 \times 10^{-14} \times AB - 2.45279 \times 10^{-13} \times AC + 5.00293 \times 10^{-13} \times AD + 3.86535 \times 10^{-16} \times BC \\ &-4.00121 \times 10^{-14} \times BD + 4.25177 \times 10^{-15} \times CD - 2.58868 \times 10^{-12} \times A^2 - 6.17202 \times 10^{-15} \times B^2 \\ &-2.09586 \times 10^{-13} \times C^2 - 8.09201 \times 10^{-14} \times D^2 \end{aligned} \quad (2)$$

(1) Analysis of Variance for the Beam Mass Response Surface Regression Model

Variance analysis of the beam mass response surface model, with the analysis results shown in Table 7.

Table 7. ANOVA of beam mass-regression model

Statistical evaluation index Numerical	value
Coefficient of determination (R^2)	0.9998
Adjusted coefficient (R_{Adj})	0.9989
Prediction coefficient (R_{pred})	0.9973
Coefficient of variation (C_v)	0.11
Signal-to-noise ratio (SNR)	166.957
Prediction error sum of squares (PRESS)	7.76×10^{-5}

From the data in the table, it can be observed that the coefficient of variation of the response surface model is relatively small, indicating that the sample data is quite reliable. The difference between the adjusted coefficient of determination and the coefficient of determination is less than 0.2, with similar values, indicating a good fit of the response surface model for regression. The model's signal-to-noise ratio is greater than 4, and the prediction error sum of squares is particularly small, demonstrating the model's high precision.

(2) Significance test for the beam mass response surface regression model.

Significance test for the beam mass response surface regression model is conducted, and the results of the test are shown in Table 8:

From the data in the table, it can be inferred that the p-value of the regression model is less than 0.005, indicating the model's significance and favorability. The F-values in the regression model are all relatively large, indicating a strong impact of the factors on the beam mass.

In the aforementioned analysis of variance, the correlation coefficients of each model are all greater than 0.99, the adjusted coefficients are also close, and the signal-to-noise ratios are all greater than 4. Furthermore, in the significance test, the p-values of the regression models are all less than 0.005, and the F-values are relatively large, indicating the significance of the model. The obtained response

surface models demonstrate high fitting accuracy, a significant regression effect, and a strong impact of the factors on the response, providing a relatively precise response surface model for beam structural design.

Table 8. Significance test table of beam mass-response surface regression model

Source	Sum of squares	Degrees of freedom	Mean square	F value	Pvalue	Significance
Model	1.378×10^6	14	9.841×10^5	6.366×10^7	< 0.0001	Highly significant
A(Bottom Plate Thickness)	9.372×10^6	1	9.372×10^6	6.366×10^7	< 0.0001	Highly significant
B(FlangeWidth)	3.947×10^5	1	3.947×10^5	6.366×10^7	< 0.0001	Highly significant
C(Main Wall Plate Thickness)	3.374×10^6	1	3.374×10^6	6.366×10^7	< 0.0001	Highly significant
D(Secondary Wall Plate Thickness)	6.374×10^5	1	6.374×10^5	6.366×10^7	< 0.0001	Highly significant
Residual	0.000	14	0.000	—	—	—
Lack of Fit	0.000	10	0.000	—	—	—
Pure Error	0.000	4	0.000	—	—	—
Total	1.378×10^7	28	—	—	—	—

Note: P<0.01 highly significant, P<0.05 significant

4.6. Multi-objective Optimization based on Genetic Algorithm (MOGA)

The information reflected by the response surface is just a reference value and has not undergone a comprehensive global comparison. The results may not necessarily be the optimal output, requiring optimization of the response surface model.

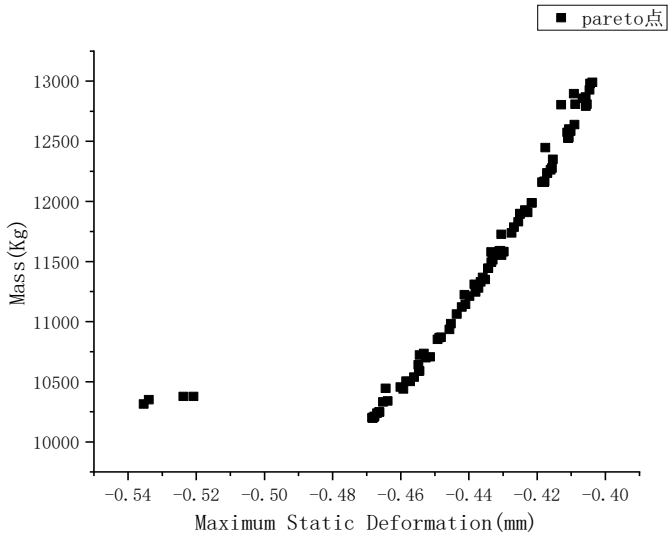

Figure 8. Pareto optimal solution set

In this paper, the Response Surface Optimization module in the Design Experiment menu of ANSYS Workbench software is utilized. The MOGA (multi-objective genetic algorithm) is selected, with an initial sample quantity of 800, a sample quantity of 100 for each iteration, and a maximum iteration quantity of 50. The Pareto optimal solution set is obtained, as shown in Figure 8, with two axes x and y representing the two optimization objectives: maximum static deformation and beam mass. The x and y objective functions jointly constitute the Pareto solution for multi-objective optimization.

Based on the boundary constraint conditions, select the most appropriate solutions from the numerous Pareto solutions as candidate points for the target functions. Select 3 sets of candidate points as shown in Table 9.

Table 9. Candidate Points

Parameter	Candidate Point 1	Candidate Point 2	Candidate Point 3
Bottom Plate Thickness (P1)/(mm)	15.018	18.3	15.3
Flange Width (P5)/(mm)	51.25	59.425	237.66
Main Wall Plate Thickness (P8)/(mm)	20.043	31.952	26.433
Secondary Wall Plate Thickness/(mm)	20.555	37.147	24.1
Maximum Static Deformation(R1)/(mm)	-0.66793	-0.63341	-0.7208
Mass(R2)/(Kg)	10203	11495	10378

Comparing the three sets of candidate points, candidate point 1 is selected as the optimal point, which is then submitted to the parameter design space for rounding and correction of the optimized parameters. The comparison of input parameters before and after optimization is shown in Table 10.

Table 10. Optimal values

Name	Bottom Plate Thickness P1/(mm)	Flange Width P5/(mm)	Main Wall Plate ThicknessP8/(mm)	Secondary Wall Plate ThicknessP9/(mm)
Optimal parameters	15.018	51.25	20.043	20.555
Corrected parameters	16	52	21	21
Initial parameters	25	200	30	30

A comparison of the numerical values before and after the optimization of the beam is shown in Table 11.

Table 11. Comparison before and after optimization

Name	Before Optimization	After Optimization	Optimization Result Percentage
Mass/(Kg)	11689	9979	14.63%
Maximum Static Deformation/(mm)	-0.717	-0.665	8.3%

From the optimization results, it can be observed that by selecting the four parameters with the highest sensitivity through parameter sensitivity analysis as design variables for optimization, there was a noticeable change in the beam mass. The optimization results were significant, with the maximum static deformation of the welded beam decreasing by 0.052mm, an 8.3% decrease compared to before optimization. The mass reduced by 1710kg, a 14.63% decrease. This has opened up avenues for designing and researching beams with a focus on lightweight construction, enabling further exploration in the pursuit of lightweight design goals.

5. SUMMARY

The research on beam structures was conducted to reduce the deflection of large-span beams, leading to the following conclusions:

(1) The bending and torsional section coefficients of beams with non-rectangular cross-sections are greater than those of rectangular beams, indicating superior bending and torsional performance of beams with non-rectangular cross-sections.

(2) Static analysis using finite elements was performed on cast beams and welded beams to compare their maximum static deformation, revealing that for large-span heavy-duty gantry machine tool beams, welding fabrication is more suitable.

(3) Multi-objective optimization of welded beams was carried out using response surface analysis. The response model was established, and its significance was verified through analysis, confirming the reliability of the model. The optimization results were significant, with a reduction of 0.052mm in maximum static deformation of the welded beam, an 8.3% decrease compared to before optimization. Additionally, the mass decreased by 1710kg, representing a 14.63% decrease.

ACKNOWLEDGMENTS

The authors gratefully acknowledge the financial support by The Innovation Fund of Postgraduate, Sichuan University of Science & Engineering (Y2022062).

REFERENCES

[1] Li Zhongtian. Design and research of large-scale seamless ring turning and milling compound processing machine tools [D]. Shandong University,2013.

[2] ZATARAIN•M, LEJARDI E, EGANA F Modular synthesis of machine tools [J]. Annals of the CIRP. 1998. 47 (1):333-336.

[3] Li Y, Lu C Structure analysis and optimization for gantry beam of guideway grinder[C]// American Institute of Physics (AIP) Conference Proceedings. Melville: AIP Publishing, 2017, 1820(1): 1-6.

[4] Guo Linna, Zheng Tianchi, Ju Jiaquan et. Design and optimization of beam structure of moving beam gantry machining center [J]. Modern Manufacturing Engineering, 2017(6): 96–99.

[5] Reddy, Agami T. Applied Data Analysis and Modeling for Energy Engineers and Scientists| Inverse Methods [J]. 2011, 10.1007/978-1-4419-9613-8(Chapter 11):327-357.

[6] Gu HaipengLightweight design of key components of .GL-2013Z gantry machining center [D]. Lanzhou University of Technology.